Original Article

Assessment of glymphatic dysfunction in pediatric idiopathic intracranial hypertension: insights from quantitative diffusivity and perivascular spaces analysis—a case-control study

Israel Cohen[1,2]^, Chen Hoffmann[1,2], Yiftach Barash[1,2]^, Ruth Lekach[2,3], Bruria Ben-Zeev[1,4], Efrat Zohar-Dayan[1,4], Shai Shrot[1,2]^

[1]Department of Diagnostic Imaging, Sheba Medical Center, Tel Hashomer, Israel; [2]Faculty of Medicine, Tel Aviv University, Tel Aviv, Israel; [3]Department of Nuclear Medicine, Tel-Aviv Sourasky Medical Center, Tel Aviv, Israel; [4]Pediatric Neurology Unit, Edmond and Lily Safra Children's Hospital, Sheba Medical Center, Ramat Gan, Israel

Contributions: (I) Conception and design: S Shrot; (II) Administrative support: S Shrot, I Cohen; (III) Provision of study materials or patients: S Shrot, I Cohen, B Ben-Zeev, E Zohar-Dayan; (IV) Collection and assembly of data: S Shrot, I Cohen, B Ben-Zeev, E Zohar-Dayan, R Lekach, Y Barash; (V) Data analysis and interpretation: S Shrot, I Cohen, R Lekach, Y Barash; (VI) Manuscript writing: All authors; (VII) Final approval of manuscript: All authors.

Correspondence to: Israel Cohen, MD. Faculty of Medicine, Tel Aviv University, Tel Aviv, Israel; Department of Diagnostic Imaging, Sheba Medical Center, Tel Hashomer, Derech Sheba 2, Ramat Gan 526200, Israel. Email: Israel.cohen@sheba.health.gov.il.

Background: The impaired drainage of cerebrospinal fluid through the glymphatic system is thought to play a role in the idiopathic intracranial hypertension (IIH) pathophysiology. Limited data exist regarding the glymphatic system's involvement in pediatric patients with IIH. Therefore, the study's objective was to quantitatively evaluate alterations in parenchymal diffusivity and magnetic resonance imaging (MRI)-visible dilated perivascular spaces (PVS) as imaging indicators of glymphatic dysfunction in pediatric patients with IIH.

Methods: Patients diagnosed with IIH in 2017–2022 in a single tertiary center (Sheba Medical Center, Israel) were retrospectively reviewed. Twenty-four pediatric patients were enrolled. All patients underwent clinical 3-T brain MRI. The control group included 24 age- and gender-matched healthy subjects with a normal-appearing brain on imaging. We used automatic atlas-based diffusion-weighted imaging analysis to determine regional diffusivity of the thalamus, caudate, putamen, globus pallidus, hippocampus, amygdala, and brain stem. PVS were evaluated using a semi-quantitative rating scale on T2-weighted images. Variables were compared using the Mann-Whitney test. Multivariate analysis of covariance was used to test for differences between controls and IIH patients.

Results: No significant differences in regional brain diffusivity were observed between individuals with IIH and healthy controls (P=0.14–0.91 for various brain regions). The number of visible PVS was comparable between patients with IIH and the control group across all evaluated sites (P=0.12–0.74 for various brain regions).

Conclusions: Pediatric IIH patients exhibited similar patterns of parenchymal diffusivity and PVS compared to age-matched controls. These findings do not support the hypothesis that the glymphatic system may play a role in the pathophysiology of pediatric IIH, although previously postulated. However, employing more sophisticated magnetic resonance (MR) techniques could enhance the sensitivity in uncovering underlying glymphatic dysfunction. Further research is warranted to validate and explore this association in

^ ORCID: Israel Cohen, 0000-0001-7447-6894; Yiftach Barash, 0000-0002-7242-1328; Shai Shrot, 0000-0001-8954-3244.

larger cohorts and investigate the underlying mechanisms involved in IIH.

Keywords: Idiopathic intracranial hypertension (IIH); glymphatic system; diffusion-weighted magnetic resonance imaging (diffusion-weighted MRI); perivascular spaces (PVS); pseudotumor cerebri

Submitted Jul 22, 2023. Accepted for publication Nov 21, 2023. Published online Jan 02, 2024.
doi: 10.21037/qims-23-1043
View this article at: https://dx.doi.org/10.21037/qims-23-1043

Introduction

Idiopathic intracranial hypertension (IIH), known as pseudotumor cerebri, is characterized by increased intracranial pressure without an identifiable cause. Increased intracranial pressure can cause headaches, blurred vision, and tinnitus (1). The exact pathogenesis of IIH is not fully understood. The pathophysiology of IIH probably involves several mechanisms, including disturbances in cerebral venous outflow dynamics, compromised cerebrospinal fluid (CSF) absorption, anomalous pulsatile CSF flow, altered venous pressure gradients, metabolic and endocrine influences, and genetic predisposition (2). In recent years, the glymphatic system has emerged as an intrinsic clearance mechanism responsible for eliminating metabolites and waste products from the brain. Impairment of the glymphatic system may contribute to the accumulation of waste products in the brain, leading to increased intracranial pressure. Such impairment was suggested to contribute to the pathogenesis of IIH (3).

Diffusion-weighted imaging (DWI), performed routinely on brain MRI, reflects the free movement of water molecules in the brain parenchyma. Apparent diffusion coefficient (ADC) values, the quantitative measure of water diffusion, improve the assessment of the parenchymal microstructure and can potentially evaluate subtle parenchymal changes not apparent in morphological magnetic resonance imaging (MRI) sequences (4). In IIH, changes in ADC values have been observed in different brain regions, including periventricular white matter (5). It is thought that the changes may be related to alterations in brain tissue water content and cellular density caused by increased intracranial pressure. There is evidence to suggest that there may be a correlation between ADC changes and glymphatic dysfunction (6,7).

Perivascular spaces (PVS) are fluid-filled spaces surrounding the small cerebral penetrating vessels and are considered an essential component of the glymphatic system. A recent study has suggested that multiple PVS on brain MRI can be an imaging biomarker for glymphatic system dysfunction (8). Adult IIH was found to be associated with an increased number of visible intracranial PVS, suggesting glymphatic dysfunction (8).

Pediatric IIH and the adult form of the disease share clinical similarities. Given the distinct variations in patient characteristics and risk factors observed especially in pre-pubertal pediatric patients compared with adolescents or adults, it is proposed that the underlying pathophysiology of IIH may differ in pediatric patients (9). Although reported in adult patients with IIH, there is limited data exist regarding the glymphatic system's involvement in pediatric patients with IIH. Therefore, the study's objective was to quantitatively evaluate alterations in parenchymal diffusivity and MRI-visible dilated PVS as imaging indicators of glymphatic function in pediatric patients with IIH. We present this article in accordance with the STROBE reporting checklist (available at https://qims.amegroups.com/article/view/10.21037/qims-23-1043/rc).

Methods

This retrospective study was conducted in accordance with the Declaration of Helsinki (as revised in 2013). The Institutional Review Board of Sheba Medical Center, Israel approved this study (No. SMC-21-8905). Individual consent for this retrospective analysis was waived.

Study design and population

We included patients diagnosed and treated with IIH, as per the definition by Friedman *et al.* (10), in our pediatric neurology clinic at Sheba Medical Center, Israel, between 2017 and 2022. Patients who had undergone brain MRI at 3.0 T, including DWI and volumetric T1-weighted images, and had available imaging data were included in the study.

Exclusion criteria were technically inadequate imaging or image-registration quality. The interval between diagnosis and neuroimaging varied among the patients.

For the control group, a retrospective computerized search was conducted in our institution's Radiology Information System (RIS) (Carestream Vue RIS) for age- and gender-matched children with a normal-appearing brain on MRI with no known neurologic, neurocognitive, or developmental deficits undergoing imaging as a standard of care for evaluation of various indications (as syncope, family history of cancers, hearing loss or cholesteatoma of the ear, strabismus or vision abnormalities, and short stature).

MRI acquisition

All patients had routine clinical MRI scans performed on 3.0-T MRI (Philips Medical Systems, Netherlands; and Siemens Healthcare, Germany), including pre-contrast and post-contrast T1-weighted images, T2-fluid attenuated inversion recovery (FLAIR), and T2-weighted images, heme-sensitive sequences (T2* gradient echo or susceptibility-weighted imaging), and DWI. The use of one of the two 3.0-T scanners was done randomly, according to machine availability. Sequences used for analysis in current studies include volumetric T1 and diffusion-weighted images (diffusivity analysis) and volumetric T1- and T2-weighted images (PVS analysis). The parameters of the magnetic resonance (MR) sequences used for image analysis are summarized in Appendix 1.

Image processing

This study employed a specialized image-processing pipeline to extract quantitative measurements of regional brain ADC values. Briefly described, in the first step of this pipeline, the Montreal Neurological Institute-152 brain atlas was nonlinearly registered to the volumetric 1-mm T1-weighted dataset, and the resulting transformation was used to warp the Harvard-Oxford subcortical atlas brain regions to the subject-specific brain anatomy. The Montreal Neurological Institute-152 brain atlas was registered to a volumetric 1-mm T1-weighted dataset using a concatenated affine and nonlinear spline transformation. The affine transformation was determined using linear interpolation and maximization of the mutual information metric. The calculated transformation (concatenated affine and b-spline) was applied to the Montreal Neurological Institute segmentation atlas to align it to the patient T1-weighted dataset. The interpolation method was changed from linear to the nearest neighbor in order to preserve the original segmentation atlas accuracy. The B0 DWI dataset was registered to the corresponding registered volumetric 1-mm T1-weighted dataset using rigid body transform. This transform was applied to the corresponding ADC map for each subject. For regional diffusion analysis, brain regions included in this brain atlas are the thalamus, caudate, putamen, globus pallidus, amygdala, hippocampus, and brain stem. An experienced observer (S.S.) checked all registration results to ensure the registration quality. The aligned brain atlas regions were then used to measure the mean ADC values in brain structures in the left and right hemispheres.

Imaging evaluation of PVS

The quantification of PVS was performed using a semi-quantitative rating scale, which has been validated by Potter *et al.* (11) and demonstrated good observer agreement. The following sites were rated by a reading radiologist (I.C., 4 years of experience): basal ganglia, centrum semiovale, and midbrain PVS. Briefly, basal ganglia and centrum semiovale PVS were rated 0 [none], 1 [1–10], 2 [11–20], 3 [21–40], and 4 [>40], and midbrain PVS were rated 0 (nonvisible) or 1 (visible). Each hemisphere was evaluated separately for basal ganglia and centrum semiovale, and the highest score from either hemisphere was taken as the overall score. T2-weighted images were used to quantify the PVS (see *Figure 1*). In each patient's case, the scores derived from the midbrain, basal ganglia, and centrum semiovale were summed to calculate a total PVS score. A subset of ten patients from each group underwent re-evaluation by the primary reader (I.C.) at a substantial time interval to assess intra-rater agreement. Additionally, inter-rater agreement was evaluated by involving a second reader (S.S., 15 years of experience) for a random sample of ten patients from each study group.

Statistical analysis

Categorical variables were expressed as numbers and percentages. Continuous variables were expressed as mean ± standard deviation (SD). The distribution of continuous variables was assessed using a histogram and Q-Q plot (Appendix 2). Ordinal and continuous variables were compared using the Mann-Whitney test. Inter- and Intra-

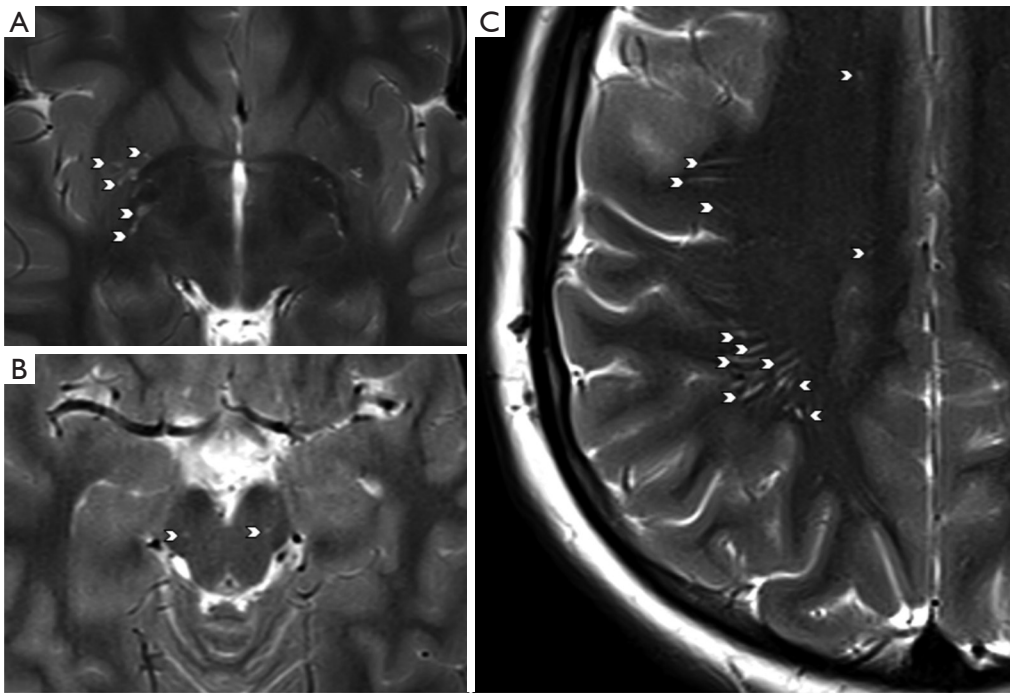

Figure 1 Axial T2-weighted magnetic resonance images highlighting PVS at different levels (indicated by arrowheads). (A) PVS at the level of the midbrain; (B) PVS at the level of the basal ganglia; (C) PVS at the level of the centrum semiovale. PVS, perivascular spaces.

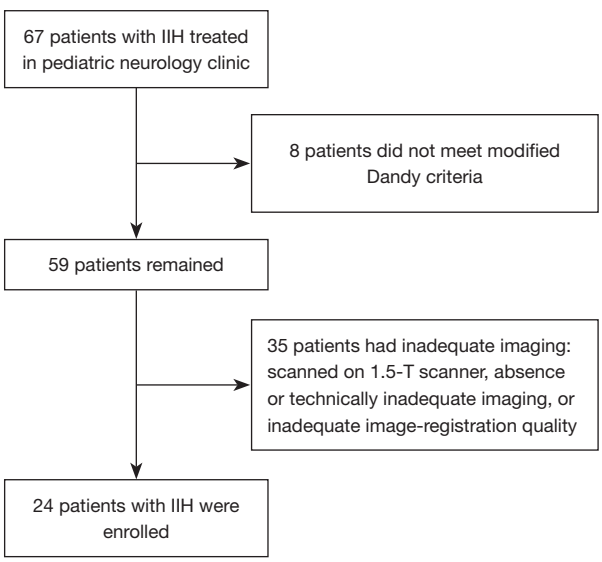

Figure 2 Flow diagram shows the enrollment of patients. IIH, idiopathic intracranial hypertension.

rater agreement was evaluated using the Cohen's kappa test. Cohen's kappa evaluates the level of agreement between the two measures, accounting for the possibility of chance agreement. The degree of agreement was categorized in accordance with previous studies as follows: poor ($\kappa \leq 0.00$), slight ($0.00 < \kappa \leq 0.20$), fair ($0.20 < \kappa \leq 0.40$), moderate ($0.40 < \kappa \leq 0.60$), substantial ($0.60 < \kappa \leq 0.80$), and nearly perfect ($0.80 < \kappa \leq 1.00$) (12). The MANCOVA analysis used the mean ADC values as dependent variables, age as a covariate, IIH group, gender and MRI scanner type as fixed factors. The correlation between PVS score and ADC values was assessed using the Spearman's rank correlation test. A two-tailed P value of <0.05 was considered statistically significant. Analyses were performed with SPSS (Version 25.0, 2019; IBM, Armonk, New York, USA).

Results

Study cohort

IIH cohort included 24 patients, with gender- and age-match healthy controls. *Figure 2* presents a flow diagram of patient enrollment. All IIH patients presented clinically with headache, which was the most common symptom, often accompanied by vision abnormalities or tinnitus. All patients had papilledema. In only a few cases, retinal hemorrhages or exudates were found. The mean opening

Table 1 Baseline demographics and clinical characteristics of IIH group

Parameters	IIH	Control
Patients (n)	24	24
Age (years), mean ± SD	12.6±3.9	13.1±3.8
Gender (n)		
Male	8	8
Female	16	16
MRI (Philips:Siemens)	17:7	20:4
Headache, n [%]	18 [75]	–
Tinnitus, n [%]	8 [33]	–
Visual abnormalities, n [%]	13 [54]	–
BMI (kg/m^2), mean ± SD	28±9	–
Papilledema, n [%]	25 [100]	–
Retinal haemorrhages, n [%]	6 [25]	–
Retinal exudates, n [%]	3 [12]	–
Vision acuity (/6), mean ± SD	–4.8±3	–
Hemoglobin level (g/dL), mean ± SD	12.4±1	–
Opening pressure (mmHg), mean ± SD	44.4±9.8	–

IIH, idiopathic intracranial hypertension; SD, standard deviation; MRI, magnetic resonance imaging; BMI, body mass index.

Table 2 Comparison of perivascular space distribution by location in IIH patients versus healthy controls

Brain region	IIH PVS (N), mean ± SD	Control PVS (N), mean ± SD	P value
Midbrain	0.7±0.5	0.8±0.4	0.74
Basal ganglia	1.0±0.2	1.0±0.2	0.64
Centrum semiovale	2.1±0.7	1.7±0.6	0.12
Total	3.8±1.0	3.5±0.9	0.26

IIH, idiopathic intracranial hypertension; PVS, perivascular spaces; N, number; SD, standard deviation.

pressure was 44.4±9.8 mmHg. The demographic features of study cohorts and clinical characteristics of the IIH group are summarized in *Table 1*.

PVS evaluation

The analysis of the weighted kappa statistic demonstrated a moderate to good level of agreement concerning PVS. Intra-rater agreement revealed substantial concordance, with values of 0.783 (P<0.001) for the midbrain, 0.667 (P=0.001) for the basal ganglia, and 0.831 (P<0.001) for the centrum semiovale. Inter-rater agreement displayed respective values of 0.490 (P=0.028), 0.571 (P=0.004), and 0.751 (P=0.001) for the midbrain, basal ganglia, and centrum semiovale.

A comparison of the overall PVS score between the IIH group and the control group using the Mann-Whitney test did not reveal a significant difference (IIH mean total: 3.8±1.0 versus controls: 3.5±0.9; P=0.26). Likewise, comparisons for each evaluated anatomical site (midbrain, basal ganglia, and centrum semiovale) also showed no significant differences (P=0.12–0.74) (*Table 2*).

ADC measurements

Mean ADC values measured in the thalamus, caudate, putamen, globus pallidus, amygdala, hippocampus, and brainstem are shown in *Figure 3* and Table S1. To account for age-related diffusivity changes, we employed a multivariate analysis of covariance (MANCOVA) analysis with the mean ADC values as dependent variables. Age was used as covariate, and IIH status, gender and MRI scanner type were included as a fixed factor. Our analysis did not reveal a statistically significant difference in ADC values between patients with IIH and healthy controls, indicating similar diffusivity between the two groups [F(7,39) =0.678, P=0.689]. No significant effect was found to gender or type of MRI magnet. Furthermore, we found no significant correlation between the PVS score and ADC measurements across the various brain regions (P values ranging from 0.09 to 0.98).

Discussion

Despite the clinical understanding of IIH, the underlying causes of the condition remain uncertain, particularly in the less explored population of pediatric patients. In recent research, the involvement of the glymphatic system in the pathophysiology has been proposed (3,8), where glymphatic overload and impaired CSF reabsorption might contribute to the development of IIH. This can potentially manifest as increased water diffusivity and prominent PVS in MRI imaging of IIH patients, indicating interstitial and perivascular fluid abnormalities. Our current study examined these two potential biomarkers related to glymphatic dysfunction in a pediatric population affected

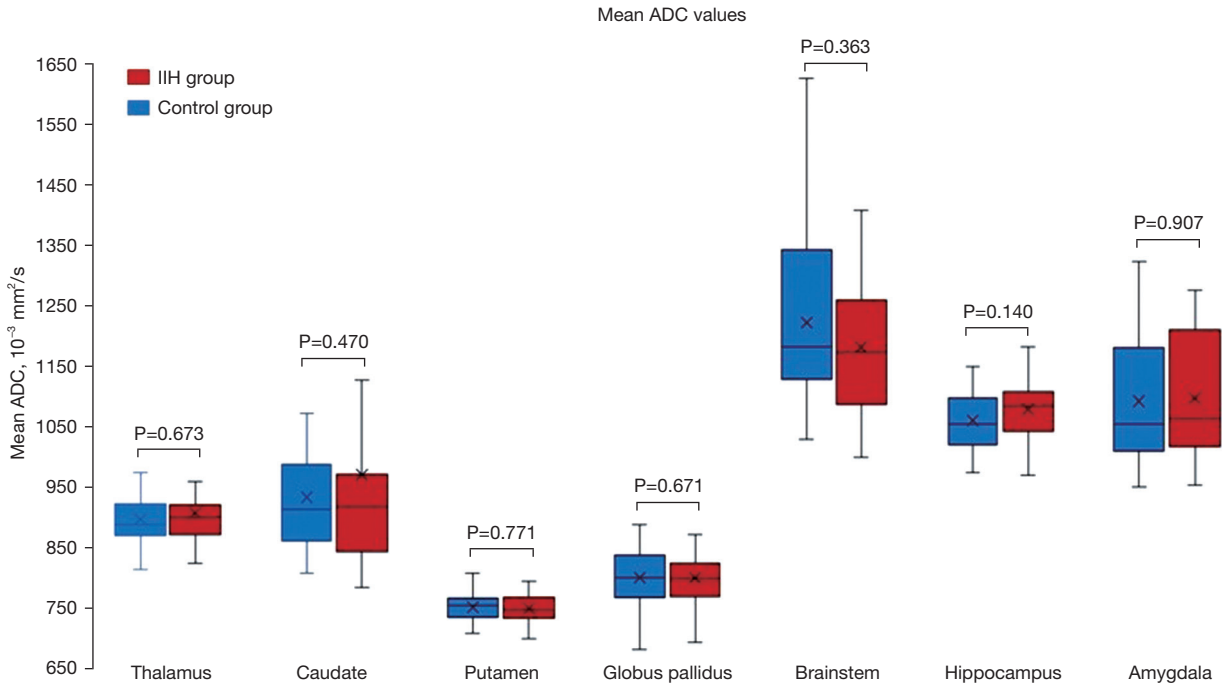

Figure 3 Comparison of mean ADC values (10^{-3} mm^2/s) in various brain regions between IIH patients and age- and gender-matched healthy controls. ADC, apparent diffusion coefficient; IIH, idiopathic intracranial hypertension.

by IIH. Our findings revealed that both parenchymal diffusivity and the presence of PVS exhibited similar patterns in pediatric IIH patients when compared to age-matched controls.

PVS can be observed in various disease conditions associated with glymphatic dysfunction, such as small-vessel disease, dementia, and multiple sclerosis (13-15). Age has been consistently identified as a significant risk factor for dilated PVS (16). Various population-based studies, including elderly and young adults, have reported positive associations between age and dilated PVS. The exact mechanism behind this age-related association is not fully understood. However, it is believed that brain atrophy and coiling of blood vessels may contribute to the dilation of PVS observed with age (17). There is limited available information on the prevalence of PVS in the pediatric population, and existing studies mainly concentrate on specific clinical groups, including individuals with headaches or epilepsy (18,19). Studies have reported a wide range of prevalence rates for dilated PVSs, varying from 3% to 100% (20-22). Considerable variation in prevalence estimates might be due to differences in the types of MRI magnet strength used, inconsistent definitions of "normal" versus "dilated" PVS, and the lack of standardized methods for quantifying the extent of visible PVS.

Lenck *et al.* have suggested that IIH might be related to glymphatic system overload (23). They hypothesized that overflow of the lymphatic CSF outflow pathway might result in venous restriction of CSF outflow. Recently, Jones *et al.* have reported an increased number of dilated PVS in adult patients with IIH compared with controls (8). However, in the current study, no difference in PVS was found in pediatric IIH patients compared with healthy controls. It may be that tissue compliance in this age group is different and, therefore, responds differently to elevated intracranial pressure compared to older individuals, whether prominent PVS is the primary cause of the increased intracranial pressure or seen as secondary to the increased pressure. Similarly, in children with IIH, some imaging features are seen in significantly lower frequencies than in adult patients (24). Our findings may also be attributed to potential differences in the underlying etiology of IIH between pediatric and adult populations. Different demographic characteristics and frequency imaging findings differ between these two groups, especially in younger pre-pubertal children (9,24), suggesting possible distinct

etiologies of IIH in pediatric and adult patients. Last, the high prevalence of PVS in healthy children, specifically when evaluated in 3.0-T magnets, might also contribute to the difference in our results compared with adult IIH (22).

Emerging evidence suggests a potential correlation between glymphatic dysfunction and changes in brain water diffusivity (7,25,26). During sleep, the glymphatic system in the brain efficiently clears waste products by facilitating the entry of CSF, resulting in increased water diffusivity in various brain regions (6). Our study found no significant difference in the ADC values between individuals with IIH and age- and gender-matched healthy controls. This suggests that despite the elevated CSF pressure, the ADC values indicated no cerebral edema-related changes. These findings are consistent with previous studies that did not observe significant alterations in brain diffusion measures in individuals with IIH (27-29). Compared to prior studies that relied on manual region-of-interest-based measurement of ADC, our study utilized automated segmentation in a relatively large IIH cohort. This approach allowed for a more comprehensive evaluation of diffusivity changes.

While pediatric IIH patients and normal controls did not display differences in terms of PVS and diffusivity measurements, a recent study by Eide *et al.* (30) employed advanced techniques and reported glymphatic disruptions in IIH patients. This involved using intrathecal gadobutrol as an MRI tracer, revealing increased tracer retention and delayed clearance in various brain regions of IIH patients, encompassing both grey and white matter. These findings imply impaired glymphatic function, which could affect metabolic waste clearance. This suggests that the parameters assessed in the present study, acquired from clinical studies, may lack the sensitivity and specificity required to uncover glymphatic disturbances in individuals with IIH.

Apart from potential altered glymphatic clearance, various pathogenic mechanisms have been suggested for IIH (2). Notably, disturbances in cerebral venous outflow dynamics and compromised CSF absorption have been posited as contributory factors in the genesis of IIH. Furthermore, deviations in CSF dynamics characterized by anomalous pulsatile CSF flow and altered venous pressure gradients are thought to compound the escalation of intracranial pressure characteristic of IIH. In addition to the aforementioned mechanistic aspects, metabolic and endocrine influences have attracted attention as potential determinants of IIH. Inflammatory mediators emanating from adipose tissue, prominently including escalated levels of leptin and various cytokines, have emerged as implicated factors in the subset of IIH cases associated with obesity. Concomitantly, hormonal actors such as incretins and glucocorticoids, alongside the renin-angiotensin system, have been proffered as candidates exerting an influence over the pathophysiology of IIH. Moreover, genetic predisposition has been broached as a contributory facet in IIH susceptibility.

Our study has several limitations that should be considered. Our study was hypothesis-generated, meaning that its primary aim was to explore quantitative imaging features in clinical imaging (PVS and parenchymal diffusivity) as potential biomarkers of glymphatic dysfunction in pediatric IIH. Nevertheless, the sample size in our study, though larger than prior studies, might not have been adequate to support our hypothesis fully. This limitation could impact our findings' statistical power and restrict the results' generalizability. Future studies should aim to include a larger and more diverse participant population to enhance the strength and validity of our conclusions. Another limitation of our study is the lack of automation in quantifying the PVS. This manual quantification method may impact the accuracy of our measurements. Utilizing automated segmentation techniques could minimize interobserver variability and enhance the precision of PVS quantification. Furthermore, there might be a slight variance in imaging quality between studies due to factors related to individual patients and technical considerations. Although we aimed to mitigate this variability by implementing a consistent imaging protocol across all patients, it is essential to acknowledge that subtle differences in image quality could still exist and potentially influence the results.

Conclusions

In conclusion, pediatric IIH patients exhibited similar patterns of parenchymal diffusivity and PVS compared to age-matched controls. These findings do not support the hypothesis that the glymphatic system may play a role in the pathophysiology of pediatric IIH, although previously postulated. However, employing more sophisticated MR techniques could enhance the sensitivity in uncovering underlying glymphatic dysfunction. Further research is warranted to validate and explore this association in larger cohorts and investigate the underlying mechanisms involved in pediatric IIH.

Acknowledgments

Funding: None.

Footnote

Reporting Checklist: The authors have completed the STROBE reporting checklist. Available at https://qims.amegroups.com/article/view/10.21037/qims-23-1043/rc

Conflicts of Interest: All authors have completed the ICMJE uniform disclosure form (available at https://qims.amegroups.com/article/view/10.21037/qims-23-1043/coif). The authors have no conflicts of interest to declare.

Ethical Statement: The authors are accountable for all aspects of the work in ensuring that questions related to the accuracy or integrity of any part of the work are appropriately investigated and resolved. This retrospective study was conducted in accordance with the Declaration of Helsinki (as revised in 2013). The institutional review board of Sheba Medical Center, Israel approved this study (No. SMC-21-8905). Individual consent for this retrospective analysis was waived.

References

1. Guarnizo A, Albreiki D, Cruz JP, Létourneau-Guillon L, Iancu D, Torres C. Papilledema: A Review of the Pathophysiology, Imaging Findings, and Mimics. Can Assoc Radiol J 2022;73:557-67.
2. Wang MTM, Bhatti MT, Danesh-Meyer HV. Idiopathic intracranial hypertension: Pathophysiology, diagnosis and management. J Clin Neurosci 2022;95:172-9.
3. Steinruecke M, Tiefenbach J, Park JJ, Kaliaperumal C. Role of the glymphatic system in idiopathic intracranial hypertension. Clin Neurol Neurosurg 2022;222:107446.
4. Koh DM, Collins DJ. Diffusion-weighted MRI in the body: applications and challenges in oncology. AJR Am J Roentgenol 2007;188:1622-35.
5. Sarica A, Curcio M, Rapisarda L, Cerasa A, Quattrone A, Bono F. Periventricular white matter changes in idiopathic intracranial hypertension. Ann Clin Transl Neurol 2019;6:233-42.
6. Demiral ŞB, Tomasi D, Sarlls J, Lee H, Wiers CE, Zehra A, Srivastava T, Ke K, Shokri-Kojori E, Freeman CR, Lindgren E, Ramirez V, Miller G, Bandettini P, Horovitz S, Wang GJ, Benveniste H, Volkow ND. Apparent diffusion coefficient changes in human brain during sleep - Does it inform on the existence of a glymphatic system? Neuroimage 2019;185:263-73.
7. Valnes LM, Mitusch SK, Ringstad G, Eide PK, Funke SW, Mardal KA. Apparent diffusion coefficient estimates based on 24 hours tracer movement support glymphatic transport in human cerebral cortex. Sci Rep 2020;10:9176.
8. Jones O, Cutsforth-Gregory J, Chen J, Bhatti MT, Huston J, Brinjikji W. Idiopathic Intracranial Hypertension is Associated with a Higher Burden of Visible Cerebral Perivascular Spaces: The Glymphatic Connection. AJNR Am J Neuroradiol 2021;42:2160-4.
9. Malem A, Sheth T, Muthusamy B. Paediatric Idiopathic Intracranial Hypertension (IIH)-A Review. Life (Basel) 2021.
10. Friedman DI, Liu GT, Digre KB. Revised diagnostic criteria for the pseudotumor cerebri syndrome in adults and children. Neurology 2013;81:1159-65.
11. Potter GM, Chappell FM, Morris Z, Wardlaw JM. Cerebral perivascular spaces visible on magnetic resonance imaging: development of a qualitative rating scale and its observer reliability. Cerebrovasc Dis 2015;39:224-31.
12. Landis JR, Koch GG. The measurement of observer agreement for categorical data. Biometrics 1977;33:159-74.
13. Doubal FN, MacLullich AM, Ferguson KJ, Dennis MS, Wardlaw JM. Enlarged perivascular spaces on MRI are a feature of cerebral small vessel disease. Stroke 2010;41:450-4.
14. Granberg T, Moridi T, Brand JS, Neumann S, Hlavica M, Piehl F, Ineichen BV. Enlarged perivascular spaces in multiple sclerosis on magnetic resonance imaging: a systematic review and meta-analysis. J Neurol 2020;267:3199-212.
15. Louveau A, Da Mesquita S, Kipnis J. Lymphatics in Neurological Disorders: A Neuro-Lympho-Vascular Component of Multiple Sclerosis and Alzheimer's Disease? Neuron 2016;91:957-73.
16. Wardlaw JM, Benveniste H, Nedergaard M, Zlokovic BV,

Mestre H, Lee H, et al. Perivascular spaces in the brain: anatomy, physiology and pathology. Nat Rev Neurol 2020;16:137-53.
17. Kim HG, Shin NY, Nam Y, Yun E, Yoon U, Lee HS, Ahn KJ. MRI-visible Dilated Perivascular Space in the Brain by Age: The Human Connectome Project. Radiology 2023;306:e213254.
18. Liu C, Habib T, Salimeen M, Pradhan A, Singh M, Wang M, Wu F, Zhang Y, Gao L, Yang G, Li X, Yang J. Quantification of visible Virchow-Robin spaces for detecting the functional status of the glymphatic system in children with newly diagnosed idiopathic generalized epilepsy. Seizure 2020;78:12-7.
19. Schick S, Gahleitner A, Wöber-Bingöl C, Wöber C, Ba-Ssalamah A, Schoder M, Schindler E, Prayer D. Virchow-Robin spaces in childhood migraine. Neuroradiology 1999;41:283-7.
20. Groeschel S, Chong WK, Surtees R, Hanefeld F. Virchow-Robin spaces on magnetic resonance images: normative data, their dilatation, and a review of the literature. Neuroradiology 2006;48:745-54.
21. Rollins NK, Deline C, Morriss MC. Prevalence and clinical significance of dilated Virchow-Robin spaces in childhood. Radiology 1993;189:53-7.
22. Piantino J, Boespflug EL, Schwartz DL, Luther M, Morales AM, Lin A, Fossen RV, Silbert L, Nagel BJ. Characterization of MR Imaging-Visible Perivascular Spaces in the White Matter of Healthy Adolescents at 3T. AJNR Am J Neuroradiol 2020;41:2139-45.
23. Lenck S, Radovanovic I, Nicholson P, Hodaie M, Krings T, Mendes-Pereira V. Idiopathic intracranial hypertension: The veno glymphatic connections. Neurology 2018;91:515-22.
24. Hartmann AJ, Soares BP, Bruce BB, Saindane AM, Newman NJ, Biousse V, Peragallo JH. Imaging Features of Idiopathic Intracranial Hypertension in Children. J Child Neurol 2017;32:120-6.
25. Alghanimy A, Martin C, Gallagher L, Holmes WM. The effect of a novel AQP4 facilitator, TGN-073, on glymphatic transport captured by diffusion MRI and DCE-MRI. PLoS One 2023;18:e0282955.
26. Andica C, Kamagata K, Takabayashi K, Kikuta J, Kaga H, Someya Y, Tamura Y, Kawamori R, Watada H, Taoka T, Naganawa S, Aoki S. Neuroimaging findings related to glymphatic system alterations in older adults with metabolic syndrome. Neurobiol Dis 2023;177:105990.
27. Bastin ME, Sinha S, Farrall AJ, Wardlaw JM, Whittle IR. Diffuse brain oedema in idiopathic intracranial hypertension: a quantitative magnetic resonance imaging study. J Neurol Neurosurg Psychiatry 2003;74:1693-6.
28. Owler BK, Higgins JN, Péna A, Carpenter TA, Pickard JD. Diffusion tensor imaging of benign intracranial hypertension: absence of cerebral oedema. Br J Neurosurg 2006;20:79-81.
29. Ulu EMK, Ince H, Terzi O. Diffusion-weighted imaging findings of brain parenchyma in pediatric pseudotumor cerebri. Medicine Science 2022;11:90-7.
30. Eide PK, Pripp AH, Ringstad G, Valnes LM. Impaired glymphatic function in idiopathic intracranial hypertension. Brain Commun 2021;3:fcab043.

Cite this article as: Cohen I, Hoffmann C, Barash Y, Lekach R, Ben-Zeev B, Zohar-Dayan E, Shrot S. Assessment of glymphatic dysfunction in pediatric idiopathic intracranial hypertension: insights from quantitative diffusivity and perivascular spaces analysis—a case-control study. Quant Imaging Med Surg 2024;14(1):653-661. doi: 10.21037/qims-23-1043

Supplementary

Appendix 1

Parameters of the magnetic resonance (MR) sequences used for image analysis

Siemens magnetic resonance imaging (MRI)

The sagittal T1-magnetization-prepared rapid gradient echo (MPRAGE) images were acquired with the following parameters: repetition time (TR) =2,200 ms, echo time (TE) =2.26 ms, inversion time (TI) =900 ms, field of view (FOV) =256×256 mm^2, flip angle =150°, matrix size =256×256 mm^2, voxel size =0.5×0.5×1 mm^3, slice thickness =1 mm. Axial T2: TR =5,000 ms, TE =100 ms, TI =900 ms, FOV =240 mm, flip angle =150°, voxel size =0.5×0.5×4 mm^3, slice thickness =4 mm. Diffusion-weighted imaging (DWI): TR/TE1/TE2 =5,970/57/97 ms, FOV =240 mm, section thickness/gap =3 mm/1 mm, voxel size: 1.3×1.3×3.0 mm^3, diffusion gradient encoding: b=0, 1,000 s/mm^2.

Philips MRI

The sagittal T1-turbo field echo (TFE) images were acquired with the following parameters: TR =6.7 ms, TE =3 ms, FOV =240×240 mm^2, flip angle =8°, matrix size =240×240 mm^2, voxel size =1×1×1 mm^3, slice thickness =1 mm. Axial T2: TR =3,399 ms, TE =100 ms, FOV =240×185 mm^2, flip angle =150°, matrix size =400×265 mm^2, voxel size =0.6×0.65×4 mm^3, section thickness/gap =4 mm/0.4 mm. DWI: TR =5,664 ms, TE =71 ms, FOV =240×240 mm^2, matrix size =160×126 mm^2, section thickness/gap =3 mm/0.3 mm, voxel size: 1.5×1.9×3.0 mm^3, diffusion gradient encoding: b=0, 1,000 s/mm^2.

Appendix 2

Assessment of normality for continuous variables using the histograms and Q-Q plots

Age (years)

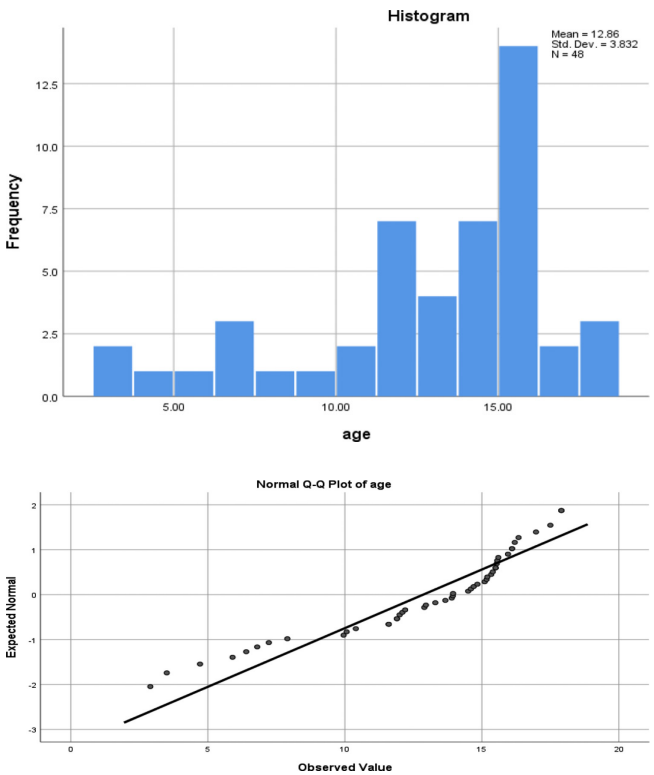

https://dx.doi.org/10.21037/qims-23-1043

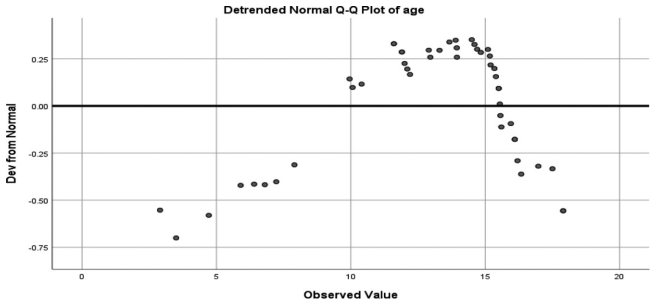

Thalamus apparent diffusion coefficient (ADC) values (mm^2/s)

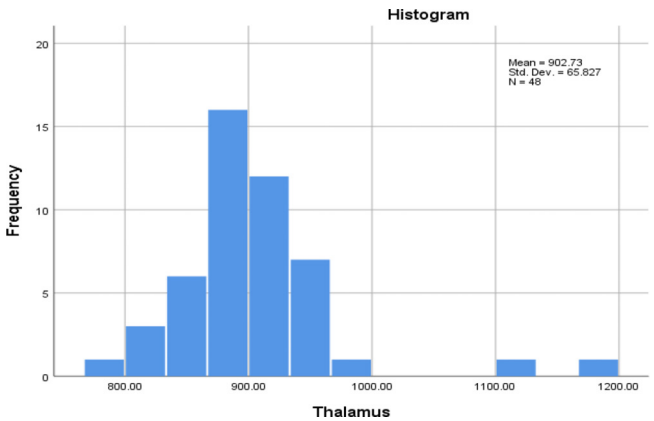

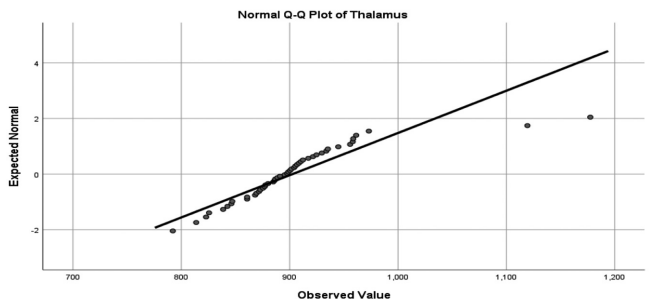

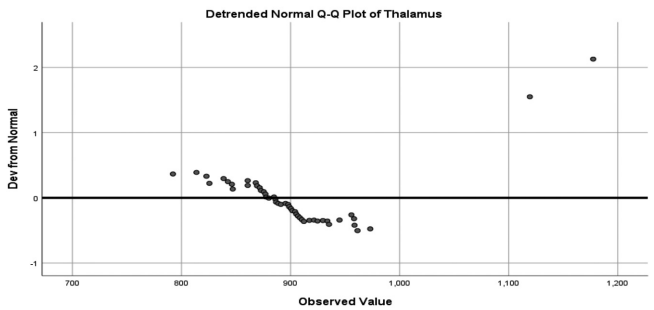

https://dx.doi.org/10.21037/qims-23-1043

Caudate ADC values (mm^2/s)

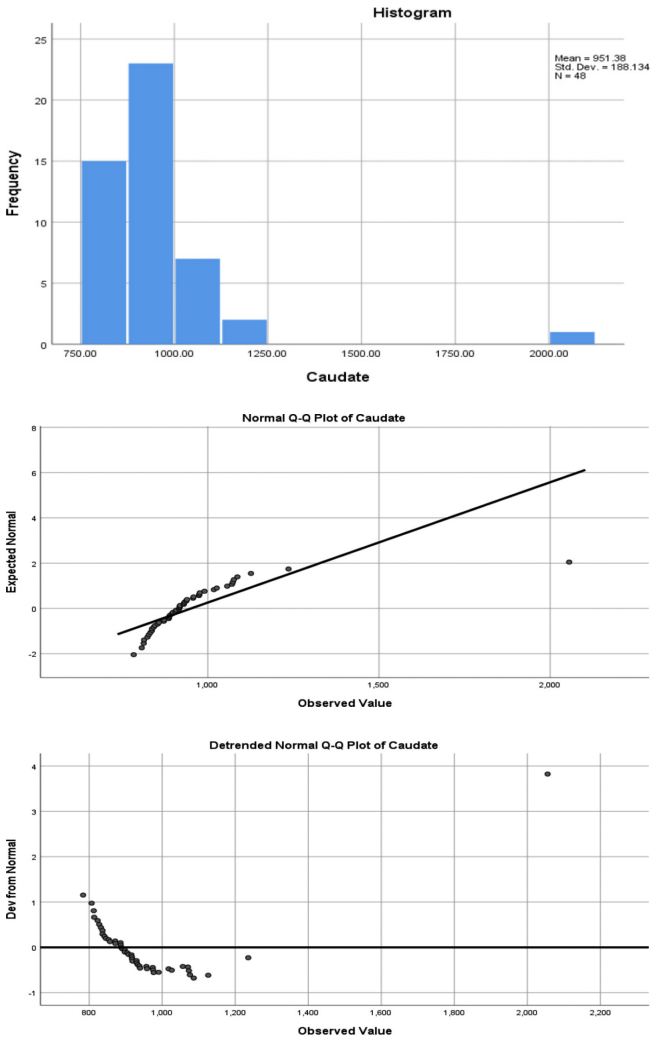

Putamen ADC values (mm^2/s)

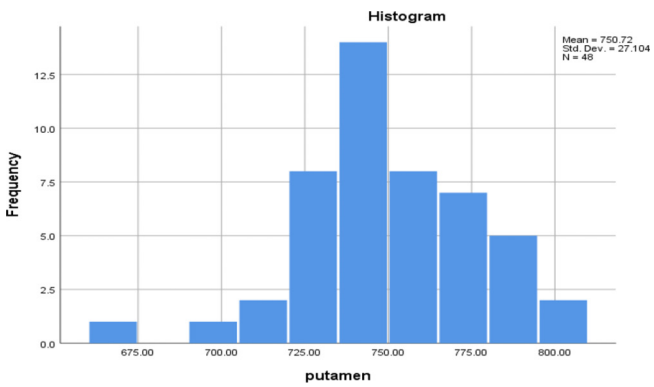

https://dx.doi.org/10.21037/qims-23-1043

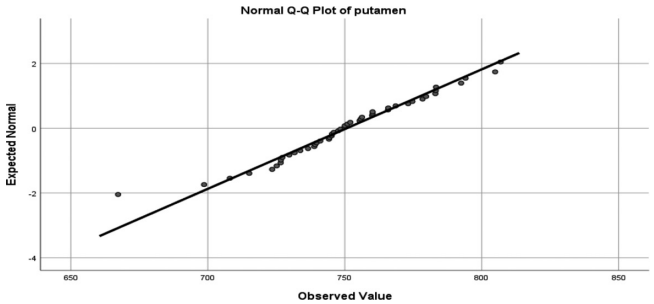

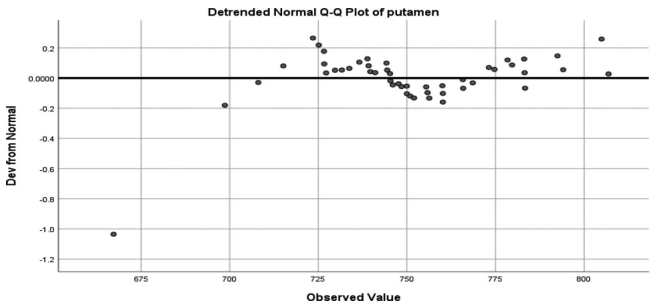

Globus pallidus (GP) ADC values (mm^2/s)

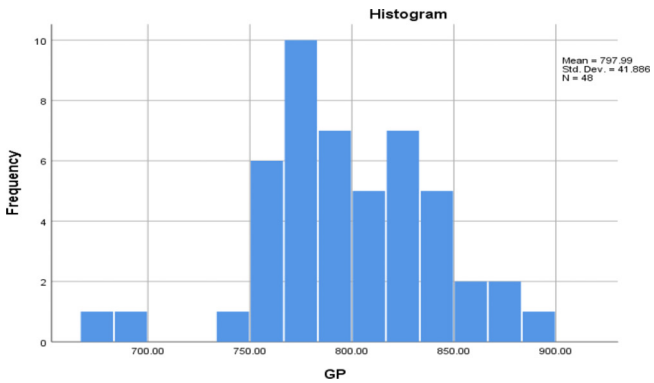

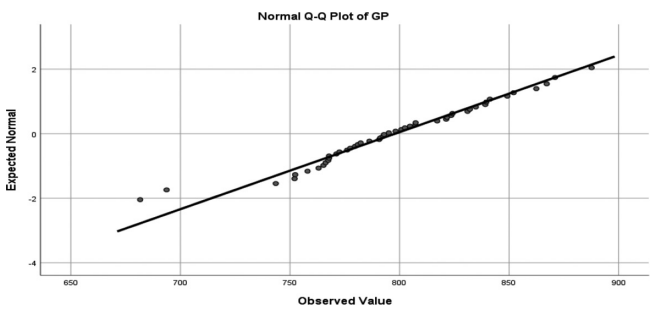

https://dx.doi.org/10.21037/qims-23-1043

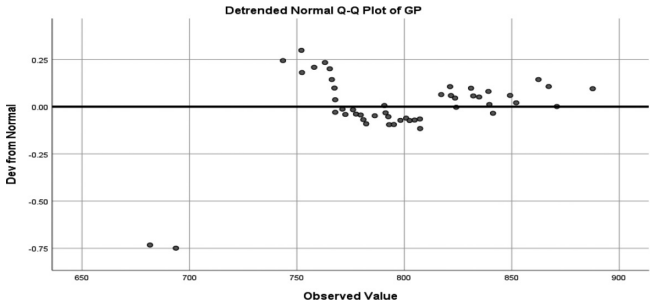

Hippocampus (HC) ADC values (mm^2/s)

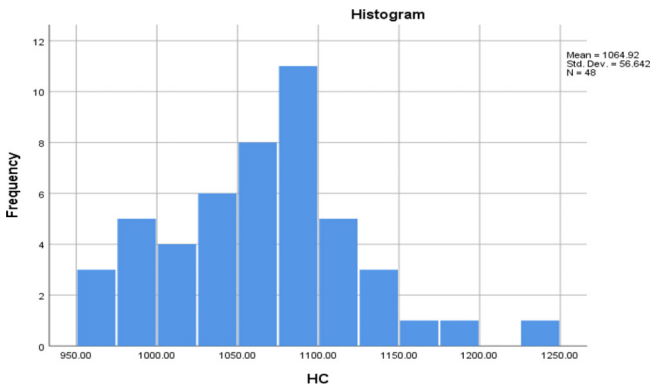

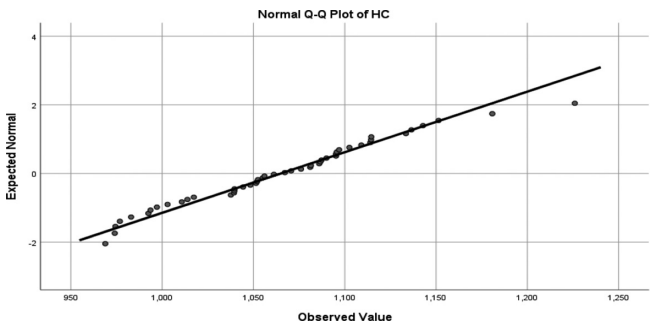

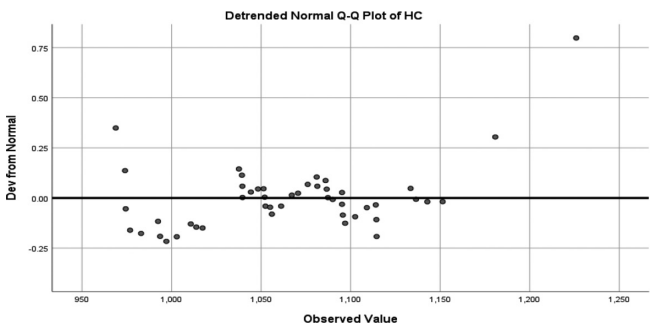

https://dx.doi.org/10.21037/qims-23-1043

Amygdala ADC values (mm^2/s)

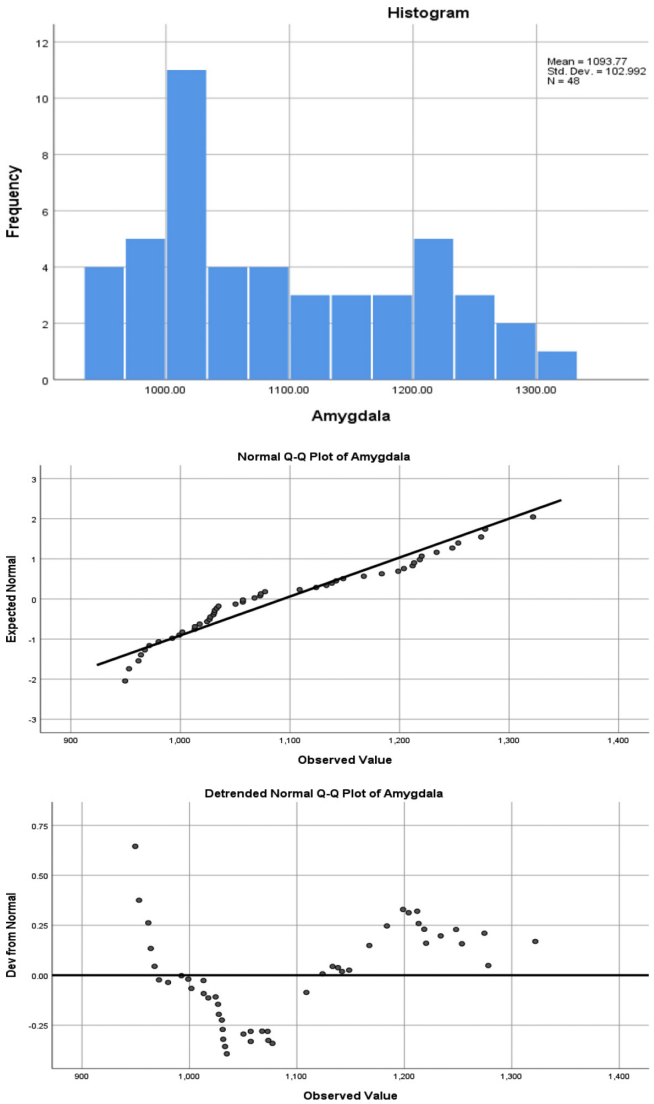

Brainstem (BS) ADC values (mm^2/s)

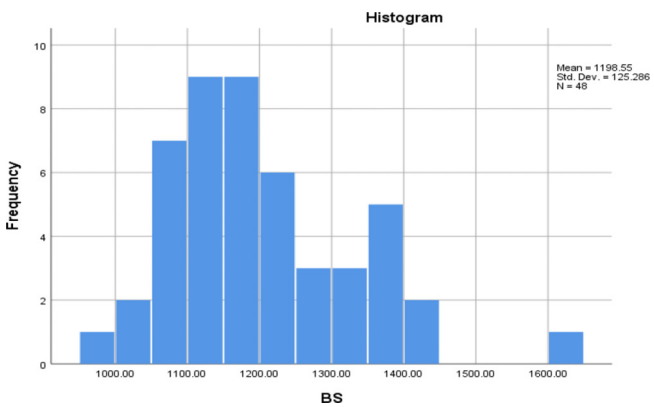

https://dx.doi.org/10.21037/qims-23-1043

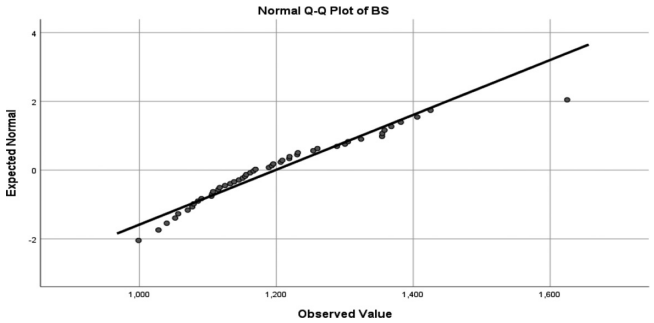

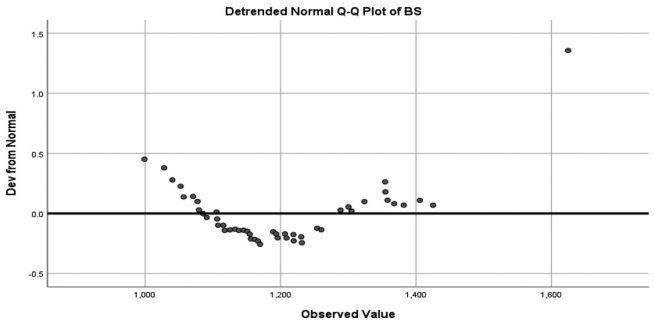

https://dx.doi.org/10.21037/qims-23-1043

Table S1 Correlation between PVS score and ADC values using Spearman's rank correlation test

PVS score/ADC values	Midbrain	Basal ganglia	Centrum semiovale
Thalamus			
Coefficient	–0.070	–0.124	–0.341
Sig. (2-tailed)	0.631	0.396	0.017
N	48	48	48
Caudate			
Coefficient	0.109	0.131	0.012
Sig. (2-tailed)	0.458	0.369	0.934
N	48	48	48
Putamen			
Coefficient	–0.026	0.212	–0.227
Sig. (2-tailed)	0.862	0.145	0.116
N	48	48	48
Globus Pallidus			
Coefficient	–0.316	0.058	0.036
Sig. (2-tailed)	0.027	0.690	0.807
N	48	48	48
Basal ganglia			
Coefficient	0.227	0.015	–0.077
Sig. (2-tailed)	0.117	0.921	0.599
N	48	48	48
Hippocampus			
Coefficient	–0.035	0.044	–0.110
Sig. (2-tailed)	0.811	0.765	0.453
N	48	48	48
Amygdala			
Coefficient	0.016	0.007	0.126
Sig. (2-tailed)	0.913	0.960	0.388
N	48	48	48

https://dx.doi.org/10.21037/qims-23-1043